Magazine of Civil Engineering

ISSN 2712-8172

journal homepage: http://engstroy.spbstu.ru/

Research article

UDC 624.04

DOI: 10.34910/MCE.134.6

Simplified finite element model for rectangular CFST columns strength calculation under eccentric compression

A. Chepurnenko ✉ , ***B. Yazyev*** , ***S. Al-Zgul*** , ***V. Tyurina***

Don State Technical University, Rostov-on-Don, Russian Federation

✉ *anton_chepurnenk@mail.ru*

Keywords: finite element method, numerical models, tubular steel structures, reinforced concrete, mechanical performance, compressive strength

Abstract. Concrete filled steel tubular (CFST) column is one of the most effective building structures types that combine high bearing capacity and economy. Three-dimensional nonlinear finite element analysis is the most common and reliable method for determining the bearing capacity of CFST columns. This approach is usually applied to individual elements and is not suitable for calculating buildings and structures with CFST elements as a single whole, due to high computational complexity. The purpose of the article is to develop a simplified model that allows reducing a three-dimensional problem of calculating a CFST column to a two-dimensional one. Rectangular CFST columns subjected to eccentric compression with eccentricity in two planes are considered. The problem dimension is reduced based on the hypothesis of plane sections. Rectangular elements are used for the concrete core and one-dimensional bar elements are used for the steel pipe. The developed model was verified by comparing calculation results with the results of three-dimensional finite element modeling in ANSYS. The maximum discrepancy between the results for stresses was 2.3 %. The model was also validated on experimental data for 38 samples presented in 3 different papers. The proposed model allows to significantly reduce the machine time costs when calculating CFST columns in a physically nonlinear formulation.

Citation: Chepurnenko, A., Yazyev, B., Al-Zgul, S., Tyurina, V. Simplified finite element model for rectangular CFST columns strength calculation under eccentric compression. Magazine of Civil Engineering. 2025. 18(2). Article no. 13406. DOI: 10.34910/MCE.134.6

1. Introduction

Concrete filled steel tubular (CFST) columns have attracted considerable attention in the construction industry due to their excellent mechanical properties, including high load-bearing capacity [1], ductility [2], and fire resistance [3]. The combined action of the steel tube and concrete core in the circumferential direction improves the compressive strength of concrete [4], making CFST columns a popular choice for high-rise buildings [5], bridges [6], and other unique structures. Accurate calculation of the CFST columns load-bearing capacity is essential to ensure the reliability of buildings and structures and optimize the design.

When calculating the bearing capacity of CFST structures, it is necessary to take into account the confinement effect of the concrete core by the steel pipe. Mander et al. [7] developed the model for confined concrete, which was adapted for CFST columns. This model was improved in the studies of Yu et al. [8] to take into account the nonlinear behavior of the confined concrete.

Numerical modeling, in particular finite element analysis (FEA), has become a powerful tool for predicting the load-bearing capacity of CFST columns [9]. This modeling can provide the detailed analysis of the structural behavior and the interaction between the steel tube and the concrete core [10]. The finite

element (FE) method allows for the consideration of complex stress-strain relationships for both steel and concrete [11], as well as the separation of the steel tube from the concrete core [12] and local buckling effects [13].

FEA of the CFST columns is usually performed in a three-dimensional setting. Ahmed et al. developed in paper [14] the 3D FE model to simulate the behavior of CFST columns of square cross-section strengthened with additional spiral reinforcement. The developed model accurately predicted the load-strain curves and failure modes. The article of authors Almasabha et al. [15] is devoted to three-dimensional modeling of CFST columns with circular cross-section under quasi-static axial compression. The emphasis in this work is on the scale effect, which has a great influence on the strength of large-diameter columns. In the article [16], three-dimensional FEA is used as a tool for studying the shear behavior of CFST columns. The developed FE models showed an average error of 12 % compared to the experimental results.

Parametric studies using nonlinear FEA allow to analyze the influence of various factors on the load-bearing capacity of CFST columns. Yadav and Chen [17] conducted a comprehensive parametric study for centrally compressed circular columns using the Abaqus software. Factors such as the diameter-to-thickness ratio of the steel pipe, the yield strength of the steel, the compressive strength of the concrete, and the slenderness coefficient of the column were considered. A similar problem was also considered in [18], but the friction coefficient between the concrete core and the steel shell was added to the factors listed above.

The authors of paper [19] studied self-stressing CFST columns using FE modeling in Abaqus. The initial self-stress value varied from 0 to 10 MPa. As a result of the parametric study, the calculation formula was proposed that allows taking into account the self-stress effect. In the paper [20], a comparative bearing capacity analysis of the round and square CFST columns with traditional reinforced concrete elements was performed. The comparison was carried out by means of laboratory experiments, as well as numerical experiments in Abaqus. The comparison results showed that the bearing capacity under axial compression for CFST columns is, on average, 1.5 times higher than that of reinforced concrete columns with the same consumption of concrete and steel.

The authors of work [21] compared the results of FE modeling with the provisions of various countries design codes for CFST columns. It was established that FEA provides more accurate results compared to empirical formulas.

Currently, machine learning methods are gaining increasing popularity in the task of predicting the bearing capacity of building structures, including CFST columns [22–24]. Unlike the theoretical and experimental approach with the selection of empirical formulas, machine learning methods allow taking into account complex nonlinear dependencies between parameters [25, 26]. However, to build reliable machine learning models, a large amount of data is required, which can only be obtained through laboratory and numerical experiments.

The conducted review shows that the FE method is the most common and effective method for determining the bearing capacity of CFST columns. At the same time, most publications are devoted to modeling the stress-strain state of individual CFST elements using three-dimensional FEA. Calculating CFST structures in a three-dimensional formulation taking into account physical nonlinearity requires large computational resources. This approach is not applicable for calculation of buildings and structures that include reinforced concrete elements as a single whole.

In [27], a simplified FE model was proposed that allows the three-dimensional problem of calculating a CFST column to be reduced to a two-dimensional problem based on the hypothesis of plane sections. This model was developed for columns of circular cross-section. The purpose of this work is to develop the proposed model for calculating rectangular CFST columns in the presence of the axial force eccentricity in two planes. Within the framework of the stated goal, the following tasks were formulated:

1. Obtaining resolving equations for determining the stress-strain state of a CFST element in a simplified two-dimensional formulation and developing a calculation algorithm.
2. Verification of the developed model by comparison with the results of three-dimensional FEA.
3. Validation of the developed model by comparison with the experimental results of other authors.

2. Methods

The calculation scheme of an eccentrically compressed CFST column with rectangular cross-section is shown in Fig. 1.

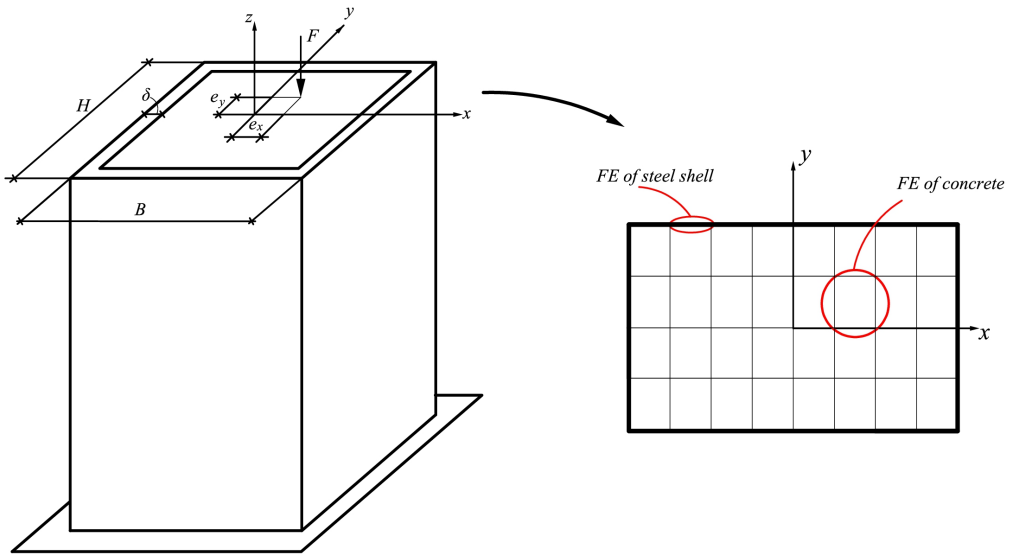

Figure 1. Calculation scheme.

Short CFST columns are considered, for which deflection does not lead to a noticeable increase in the bending moment. According to Russian design codes SR 266.1325800.2016, columns are considered short if their slenderness (the ratio of the calculated length to the radius of gyration of the reduced cross section) does not exceed 14.

When constructing the resolving equations for determining the stress-strain state of a CFST element, we will take into account the stresses σ_z in the direction of the column axis, as well as the stresses σ_x, σ_y and τ_{xy} in the plane of the cross section. Stresses τ_{xz} and τ_{yz} will be neglected. A simplified calculation method is based on the hypothesis of plane sections. In accordance with this method, the deformation along the z axis under the combined action of bending moments in two planes and axial forces can be represented as:

$$\varepsilon_z = \varepsilon_z^0 + y\chi_1 + x\chi_2. \tag{1}$$

The first term in formula (1) represents the axial deformation, the second and third terms include changes in element curvature χ_1 and χ_2.

When using the plane sections hypothesis, local effects at the ends of the CFST element are neglected, assuming that the load is transmitted through a rigid stamp.

Let us obtain the relationship between the internal forces (axial force N, bending moments M_x and M_y) and generalized deformations ε_z^0, χ_1 and χ_2. The physical equations for concrete, establishing the relationship between stresses and deformations, have the form:

$$\varepsilon_x = \frac{1}{E}\left(\sigma_x - \nu\left(\sigma_y + \sigma_z\right)\right) + \varepsilon_x^*; \tag{2}$$

$$\varepsilon_y = \frac{1}{E}\left(\sigma_y - \nu\left(\sigma_x + \sigma_z\right)\right) + \varepsilon_y^*; \tag{3}$$

$$\varepsilon_z = \frac{1}{E}\left(\sigma_z - \nu\left(\sigma_y + \sigma_x\right)\right) + \varepsilon_z^*; \tag{4}$$

$$\gamma_{xy} = \frac{2\left(1+\nu\right)}{E}\tau_{xy} + \gamma_{xy}^*, \tag{5}$$

where E is the concrete modulus of elasticity, ν is the Poisson's ratio of concrete, ε_x^*, ε_y^*, ε_z^* and γ_{xy}^* are the additional terms that may include creep deformations, shrinkage, dilatation deformations, temperature deformations, etc.

Quantities ε_x^*, ε_y^*, ε_z^* and γ_{xy}^* will be referred hereinafter to forced deformations. To be able to take into account physical nonlinearity, the modulus of elasticity E in formulas (2)–(5) is taken as a function of coordinates x and y.

The stress σ_z can be expressed from (4) as:

$$\sigma_z = E\left(\varepsilon_z - \varepsilon_z^*\right) + \nu\left(\sigma_y + \sigma_x\right) = E\left(\varepsilon_z^0 + y\chi_1 + x\chi_2 - \varepsilon_z^*\right) + \nu\left(\sigma_y + \sigma_x\right). \quad (6)$$

The physical equations for a steel shell are written as:

$$\varepsilon_{s\theta} = \frac{1}{E_s}\left(\sigma_{s\theta} - \nu_s\sigma_{sz}\right); \quad (7)$$

$$\varepsilon_{sz} = \frac{1}{E_s}\left(\sigma_{sz} - \nu_s\sigma_{s\theta}\right), \quad (8)$$

where E_s and ν_s are respectively, the modulus of elasticity and Poisson's ratio of steel.

Let us express from (7), (8) the stresses in the steel pipe through deformations:

$$\sigma_{sz} = \frac{E_s}{1-\nu_s^2}\left(\varepsilon_{sz} + \nu_s\varepsilon_{s\theta}\right); \quad (9)$$

$$\sigma_{s\theta} = \frac{E_s}{1-\nu_s^2}\left(\varepsilon_{s\theta} + \nu_s\varepsilon_{sz}\right). \quad (10)$$

It is assumed in the calculation that there is no slippage between the steel pipe and the concrete core. This hypothesis is usually fulfilled, since when designing CFST concrete columns, engineers strive to ensure a reliable connection between the steel pipe and the concrete core by welding on short periodic profile steel bars from the inside, or by using concrete on prestressing cement, which creates initial lateral compression stresses. Also, the support nodes are usually designed in such a way that the forces are transmitted simultaneously to the concrete core and the steel pipe.

From the condition of the concrete core and the steel shell joint work in z axis direction, deformation ε_{sz} at the point in the pipe with coordinates $\left(x_s; y_s\right)$ can be written as:

$$\varepsilon_{sz} = \varepsilon_z^0 + y_s\chi_1 + x_s\chi_2. \quad (11)$$

Substitution of ε_{sz} from (11), as well as $\varepsilon_{s\theta}$ from (7) into the equation (10) leads to the equation:

$$\sigma_{sz} = E_s\left(\varepsilon_z^0 + y_s\chi_1 + x_s\chi_2\right) + \nu_s\sigma_{s\theta}. \quad (12)$$

Internal forces in a column represent the sum of the forces perceived by concrete and steel:

$$N = N_s + N_b = \int\limits_{A_s} \sigma_{sz}dA + \int\limits_{A_b} \sigma_z dA; \quad (13)$$

$$M_x = M_{sx} + M_{bx} = \int\limits_{A_s} \sigma_{sz}ydA + \int\limits_{A_b} \sigma_z ydA; \quad (14)$$

$$M_y = M_{sy} + M_{by} = \int\limits_{A_s} \sigma_{sz}xdA + \int\limits_{A_b} \sigma_z xdA, \quad (15)$$

where A_b and A_s are respectively the cross-sectional areas of the concrete core and the steel shell.

The relationships between generalized deformations ε_z^0, χ_1, χ_2 and internal forces M_x, M_y, N can be obtained by substitution of (6) and (12) into (13)–(15):

$$\begin{Bmatrix} N \\ M_x \\ M_y \end{Bmatrix} = \begin{Bmatrix} N \\ N \cdot e_y \\ N \cdot e_x \end{Bmatrix} = \begin{bmatrix} EA & ES_x & ES_y \\ ES_x & EI_x & EI_{xy} \\ ES_y & EI_{xy} & EI_y \end{bmatrix} \begin{Bmatrix} \varepsilon_z^0 \\ \chi_1 \\ \chi_2 \end{Bmatrix} - \begin{Bmatrix} N^* \\ M_x^* \\ M_y^* \end{Bmatrix}, \quad (16)$$

where

$$EA = \int_{A_s} E_s(x,y)\,dA + \int_{A_b} E(x,y)\,dA; \quad (17)$$

$$ES_x = \int_{A_s} E_s(x,y)\,y\,dA + \int_{A_b} E(x,y)\,y\,dA; \quad (18)$$

$$ES_y = \int_{A_s} E_s(x,y)\,x\,dA + \int_{A_b} E(x,y)\,x\,dA; \quad (19)$$

$$EI_x = \int_{A_s} E_s(x,y)\,y^2\,dA + \int_{A_b} E(x,y)\,y^2\,dA; \quad (20)$$

$$EI_y = \int_{A_s} E_s(x,y)\,x^2\,dA + \int_{A_b} E(x,y)\,x^2\,dA; \quad (21)$$

$$EI_{xy} = \int_{A_s} E_s(x,y)\,xy\,dA + \int_{A_b} E(x,y)\,xy\,dA; \quad (22)$$

$$N^* = \int_{A_b} \left(E(x,y)\varepsilon_z^* + \nu\left(\sigma_x + \sigma_y\right)\right)dA + \nu_s \int_{A_s} \sigma_{s\theta}\,dA; \quad (23)$$

$$M_x^* = \int_{A_b} \left(E(x,y)\varepsilon_z^* + \nu\left(\sigma_x + \sigma_y\right)\right)y\,dA + \nu_s \int_{A_s} \sigma_{s\theta} y_s\,dA; \quad (24)$$

$$M_y^* = \int_{A_b} \left(E(x,y)\varepsilon_z^* + \nu\left(\sigma_x + \sigma_y\right)\right)x\,dA + \nu_s \int_{A_s} \sigma_{s\theta} x_s\,dA. \quad (25)$$

To determine the stresses acting in the plane of the cross section, the concrete core is divided into rectangular FEs, and the steel shell is modeled by one-dimensional bar elements (Fig. 2). Rounding of corners in rectangular bent-welded sections will be neglected.

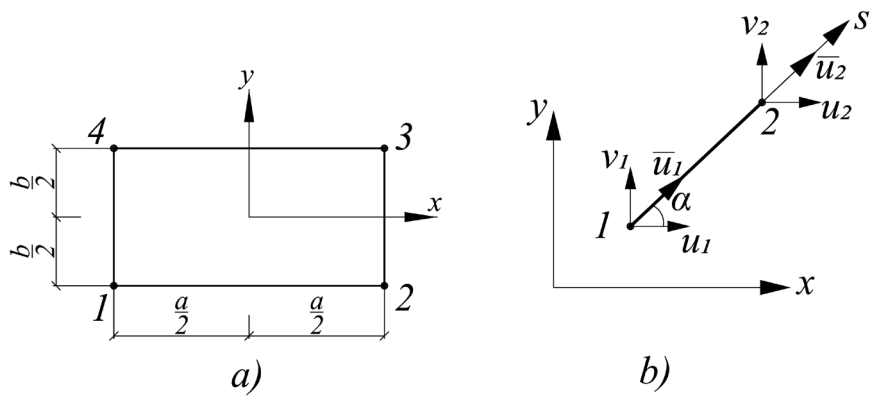

Figure 2. Finite elements for determining the stress-strain state in the plane of the cross-section: a) finite element of the concrete core, b) finite element of the steel shell.

The FE of the concrete core has 2 degrees of freedom at the node: displacements u and v in the plane of the cross section.

Approximation of displacements u and v is taken in the form:

$$u = \alpha_1 + \alpha_2 x + \alpha_3 y + \alpha_4 xy; \tag{26}$$

$$v = \beta_1 + \beta_2 x + \beta_3 y + \beta_4 xy. \tag{27}$$

Expressions (26), (27) in matrix form have the form:

$$\begin{Bmatrix} u \\ v \end{Bmatrix} = \begin{bmatrix} 1 & x & y & xy & 0 & 0 & 0 & 0 \\ 0 & 0 & 0 & 0 & 1 & x & y & xy \end{bmatrix} \{\alpha\}, \tag{28}$$

where $\{\alpha\} = \{\alpha_1 \ \alpha_2 \ \alpha_3 \ \alpha_4 \ \beta_1 \ \beta_2 \ \beta_3 \ \beta_4\}^T$.

The vector $\{\alpha\}$ can be found by substituting the coordinates of the nodes into (28):

$$\begin{bmatrix} 1 & -\frac{a}{2} & -\frac{b}{2} & \frac{ab}{4} & 0 & 0 & 0 & 0 \\ 0 & 0 & 0 & 0 & 1 & -\frac{a}{2} & -\frac{b}{2} & \frac{ab}{4} \\ 1 & \frac{a}{2} & -\frac{b}{2} & -\frac{ab}{4} & 0 & 0 & 0 & 0 \\ 0 & 0 & 0 & 0 & 1 & \frac{a}{2} & -\frac{b}{2} & -\frac{ab}{4} \\ 1 & \frac{a}{2} & \frac{b}{2} & \frac{ab}{4} & 0 & 0 & 0 & 0 \\ 0 & 0 & 0 & 0 & 1 & \frac{a}{2} & \frac{b}{2} & \frac{ab}{4} \\ 1 & -\frac{a}{2} & \frac{b}{2} & -\frac{ab}{4} & 0 & 0 & 0 & 0 \\ 0 & 0 & 0 & 0 & 1 & -\frac{a}{2} & \frac{b}{2} & -\frac{ab}{4} \end{bmatrix} \{\alpha\} = [\Phi]\{\alpha\} = \{U\}, \tag{29}$$

where $\{U\} = \{u_1 \ v_1 \ u_2 \ v_2 \ u_3 \ v_3 \ u_4 \ v_4\}^T$ is the vector of nodal displacements in the plane of the cross section.

The vector $\{\alpha\}$ is expressed from (29) as: $\{\alpha\} = [\Phi]^{-1}\{U\}$. The matrix $[\Phi]^{-1}$ has the form:

$$\left[\Phi\right]^{-1}=\begin{bmatrix}\frac{1}{4} & 0 & \frac{1}{4} & 0 & \frac{1}{4} & 0 & \frac{1}{4} & 0\\ -\frac{1}{2a} & 0 & \frac{1}{2a} & 0 & \frac{1}{2a} & 0 & -\frac{1}{2a} & 0\\ -\frac{1}{2b} & 0 & -\frac{1}{2b} & 0 & \frac{1}{2b} & 0 & \frac{1}{2b} & 0\\ \frac{1}{ab} & 0 & -\frac{1}{ab} & 0 & \frac{1}{ab} & 0 & -\frac{1}{ab} & 0\\ 0 & \frac{1}{4} & 0 & \frac{1}{4} & 0 & \frac{1}{4} & 0 & \frac{1}{4}\\ 0 & -\frac{1}{2a} & 0 & -\frac{1}{2a} & 0 & -\frac{1}{2a} & 0 & -\frac{1}{2a}\\ 0 & -\frac{1}{2b} & 0 & -\frac{1}{2b} & 0 & \frac{1}{2b} & 0 & \frac{1}{2b}\\ 0 & \frac{1}{ab} & 0 & -\frac{1}{ab} & 0 & \frac{1}{ab} & 0 & -\frac{1}{ab}\end{bmatrix}. \tag{30}$$

The deformation vector in the cross-sectional plane is determined as follows:

$$\left\{\varepsilon\right\}=\begin{Bmatrix}\frac{\partial u}{\partial x}\\ \frac{\partial v}{\partial y}\\ \frac{\partial u}{\partial y}+\frac{\partial v}{\partial x}\end{Bmatrix}=\begin{bmatrix}0 & 1 & 0 & y & 0 & 0 & 0 & 0\\ 0 & 0 & 0 & 0 & 0 & 0 & 1 & x\\ 0 & 0 & 1 & x & 0 & 1 & 0 & y\end{bmatrix}\left\{\alpha\right\}= \tag{31}$$

$$=\begin{bmatrix}0 & 1 & 0 & y & 0 & 0 & 0 & 0\\ 0 & 0 & 0 & 0 & 0 & 0 & 1 & x\\ 0 & 0 & 1 & x & 0 & 1 & 0 & y\end{bmatrix}\left[\Phi\right]^{-1}\left\{U\right\}=\left[B\right]\left\{U\right\},$$

where

$$\left[B\right]=\frac{1}{ab}\begin{bmatrix}y-\frac{b}{2} & 0 & \frac{b}{2}-y & 0 & \frac{b}{2}+y & 0 & -\frac{b}{2}-y & 0\\ 0 & x-\frac{a}{2} & 0 & -\frac{a}{2}-x & 0 & \frac{a}{2}+x & 0 & \frac{a}{2}-x\\ x-\frac{a}{2} & y-\frac{b}{2} & -\frac{a}{2}-x & \frac{b}{2}-y & \frac{a}{2}+x & \frac{b}{2}+y & \frac{a}{2}-x & -\frac{b}{2}-y\end{bmatrix}. \tag{32}$$

Next, the relationships will be obtained that allow determining the stress-strain state in the plane of the column cross-section. To do this, the quantity σ_z should be excluded from equations (2)–(4). Substitution of the equation (6) into the equations in (2)–(3) leads to the following expressions:

$$\varepsilon_x=\frac{1}{E_1}\left(\sigma_x-\nu_1\sigma_y\right)+\varepsilon_x^*-\nu\left(\varepsilon_z^0+y\chi_1+x\chi_2-\varepsilon_z^*\right); \tag{33}$$

$$\varepsilon_y=\frac{1}{E_1}\left(\sigma_y-\nu_1\sigma_x\right)+\varepsilon_y^*-\nu\left(\varepsilon_z^0+y\chi_1+x\chi_2-\varepsilon_z^*\right), \tag{34}$$

where $E_1=E/\left(1-\nu\right),\ \nu_1=\nu/\left(1-\nu\right).$

The equality in (5) can be represented as:

$$\gamma_{xy} = \frac{2(1+\nu_1)}{E_1}\tau_{xy} + \gamma^*_{xy}. \quad (35)$$

The stresses in the concrete core are expressed from (33)–(35) through the deformations in the form:

$$\sigma_x = \frac{E_1}{1-\nu_1^2}\left(\varepsilon_x + \nu_1\varepsilon_y - \left(\varepsilon^*_x + \nu_1\varepsilon^*_y\right) + \nu_1\left(\varepsilon^0_x + y\chi_1 + x\chi_2 - \varepsilon^*_z\right)\right); \quad (36)$$

$$\sigma_y = \frac{E_1}{1-\nu_1^2}\left(\varepsilon_y + \nu_1\varepsilon_x - \left(\varepsilon^*_y + \nu_1\varepsilon^*_x\right) + \nu_1\left(\varepsilon^0_z + y\chi_1 + x\chi_2 - \varepsilon^*_z\right)\right); \quad (37)$$

$$\tau_{xy} = \frac{E_1}{2(1+\nu_1)}\left(\gamma_{xy} - \gamma^*_{xy}\right). \quad (38)$$

Equalities (36)–(38) can be represented in matrix form:

$$\{\sigma\} = [D]\left(\{\varepsilon\} - \{\varepsilon^*\}\right) + \{\sigma_1\}, \quad (39)$$

where $[D] = \frac{E_1}{1-\nu_1^2}\begin{bmatrix} 1 & \nu_1 & 0 \\ \nu_1 & 1 & 0 \\ 0 & 0 & \frac{1-\nu_1}{2} \end{bmatrix}$, $\{\sigma\} = \begin{Bmatrix} \sigma_x \\ \sigma_y \\ \tau_{xy} \end{Bmatrix}$, $\{\sigma\} = \begin{Bmatrix} \sigma_x \\ \sigma_y \\ \tau_{xy} \end{Bmatrix}$, $\{\varepsilon\} = \begin{Bmatrix} \varepsilon_x \\ \varepsilon_y \\ \gamma_{xy} \end{Bmatrix}$, $\{\varepsilon^*\} = \begin{Bmatrix} \varepsilon^*_x \\ \varepsilon^*_y \\ \gamma^*_{xy} \end{Bmatrix}$,

$$\{\sigma_1\} = \frac{E_1\nu_1}{1-\nu_1^2}\left(\varepsilon^0_z + y\chi_1 + x\chi_2 - \varepsilon^*_z\right)\begin{Bmatrix} 1 \\ 1 \\ 0 \end{Bmatrix}.$$

Formula (6) can be written as:

$$\sigma_z = E\left(\varepsilon^0_z + y\chi_1 + x\chi_2 - \varepsilon^*_z\right) + \nu\{\sigma\}^T\begin{Bmatrix} 1 \\ 1 \\ 0 \end{Bmatrix}. \quad (40)$$

The resolving equations of the FE method for determining the stress-strain state in the plane of the cross section can be obtained based on the Lagrange variational principle. The potential strain energy of a CFST structure consists of the concrete core potential energy Π_b and the steel shell potential energy Π_s. The value Π_b is determined by the formula:

$$\prod_b = \frac{1}{2}\int_{A_b}\left(\sigma_x\varepsilon^{el}_x + \sigma_y\varepsilon^{el}_y + \tau_{xy}\gamma^{el}_{xy} + \sigma_z\varepsilon^{el}_z\right)dA. \quad (41)$$

The indices "el" in formula (41) correspond to elastic deformations. They are calculated as the difference between the total and forced deformations. The potential strain energy of the concrete core (41) can be represented as:

$$\prod_b = \frac{1}{2}\int_{A_b}\sigma_z\left(\varepsilon^0_z + y\chi_1 + x\chi_2 - \varepsilon^*_z\right)dA + \frac{1}{2}\int_{A_b}\{\sigma\}^T\left(\{\varepsilon\} - \{\varepsilon^*\}\right)dA. \quad (42)$$

The first integral in (42) can be represented in the following form:

$$\frac{1}{2}\int_{A_b}\sigma_z\left(\varepsilon_z^0+y\chi_1+x\chi_2-\varepsilon_z^*\right)dA=\frac{1}{2}\int_{A_b}E\left(\varepsilon_z^0+y\chi_1+x\chi_2-\varepsilon_z^*\right)^2dA+$$
$$+\frac{\nu}{2}\int_{A_b}\{\sigma\}^T\begin{Bmatrix}1\\1\\0\end{Bmatrix}\left(\varepsilon_z^0+y\chi_1+x\chi_2-\varepsilon_z^*\right)dA. \quad (43)$$

After differentiation with respect to the vector of nodal displacements $\{U\}$ to find the minimum of the total energy, the first term in (43) vanishes. The second term in (43) can be written as:

$$\frac{\nu}{2}\int_{A_b}\{\sigma\}^T\begin{Bmatrix}1\\1\\0\end{Bmatrix}\left(\varepsilon_z^0+y\chi_1+x\chi_2-\varepsilon_z^*\right)dA=$$
$$=\frac{\nu}{2}\int_{A_b}\left(\{\sigma_1\}^T+\left(\{\varepsilon\}^T-\{\varepsilon^*\}^T\right)[D]\right)\begin{Bmatrix}1\\1\\0\end{Bmatrix}\left(\varepsilon_z^0+y\chi_1+x\chi_2-\varepsilon_z^*\right)dA=$$
$$=\frac{\nu}{2}\left(\int_{A_b}\left(\{\sigma_1\}^T-\{\varepsilon^*\}^T[D]\right)\begin{Bmatrix}1\\1\\0\end{Bmatrix}\left(\varepsilon_z^0+y\chi_1+x\chi_2-\varepsilon_z^*\right)dA+\right.$$
$$\left.+\int_{A_b}\{U\}^T[B]^T[D]\begin{Bmatrix}1\\1\\0\end{Bmatrix}\left(\varepsilon_z^0+y\chi_1+x\chi_2-\varepsilon_z^*\right)dA\right). \quad (44)$$

The first integral in (44) also vanishes when differentiated with respect to $\{U\}$. When calculating the second integral, the simplifying assumption is introduced that the forced deformation ε_z^* does not change within the FE. This hypothesis is justified if the FE mesh is dense enough. Taking into account the adopted simplification, the second integral in (43) is represented as:

$$\frac{\nu}{2}\int_{A_b}\{U\}^T[B]^T[D]\begin{Bmatrix}1\\1\\0\end{Bmatrix}\left(\varepsilon_z^0+y\chi_1+x\chi_2-\varepsilon_z^*\right)dA=$$
$$=\frac{\nu}{2}\{U\}^T[B]^T[D]\begin{Bmatrix}1\\1\\0\end{Bmatrix}\left(\left(\varepsilon_z^0-\varepsilon_z^*\right)A+\chi_1\int_{A_b}ydA+\chi_2\int_{A_b}xdA\right)=$$
$$=\frac{1}{2}\{U\}^T[B]^T\,A_b\cdot\nu[D]\begin{Bmatrix}1\\1\\0\end{Bmatrix}\left(\varepsilon_z^0+y_c\chi_1+x_c\chi_2-\varepsilon_z^*\right)=$$
$$=\frac{1}{2}\{U\}^T[B]^T\,A_b\frac{E_1\nu_1}{1-\nu_1^2}\begin{Bmatrix}1\\1\\0\end{Bmatrix}\left(\varepsilon_z^0+y_c\chi_1+x_c\chi_2-\varepsilon_z^*\right)=\frac{1}{2}\{U\}^T[B]^T\,A_b\{\sigma_1\}. \quad (45)$$

Quantities x_c and y_c in formula (45) represent the coordinates of the FE center of gravity.

Let us further expand the second integral in (42):

$$\frac{1}{2}\int_{A_b}\{\sigma\}^T\left\{\varepsilon^{el}\right\}dA=\frac{1}{2}\int_{A_b}\left[\left(\{\varepsilon\}^T-\left\{\varepsilon^*\right\}^T\right)[D]+\{\sigma_1\}^T\right]\left(\{\varepsilon\}-\left\{\varepsilon^*\right\}\right)dA=$$
$$=\frac{1}{2}\int_{A_b}\{\varepsilon\}^T[D]\{\varepsilon\}-2\{\varepsilon\}^T[D]\left\{\varepsilon^*\right\}+\left\{\varepsilon^*\right\}^T[D]\left\{\varepsilon^*\right\}+\{\sigma_1\}^T\{\varepsilon\}-\{\sigma_1\}^T\left\{\varepsilon^*\right\}dA. \quad (46)$$

The terms $\left\{\varepsilon^*\right\}^T[D]\left\{\varepsilon^*\right\}$ and $\{\sigma_1\}^T\left\{\varepsilon^*\right\}$ vanish when differentiated with respect to the vector $\{U\}$. Let us separately expand the remaining terms:

$$\frac{1}{2}\int_{A_b}\{\varepsilon\}^T[D]\{\varepsilon\}dA=\frac{1}{2}\{U\}^T[B]^T[D][B]A_b\{U\}=\frac{1}{2}\{U\}^T[K_b]\{U\}, \quad (47)$$

where $[K_b]=[B]^T[D][B]A_b$ is the stiffness matrix of the concrete core FE.

$$\frac{1}{2}\int_{A_b}\{\sigma_1\}^T\{\varepsilon\}dA=\frac{1}{2}\int_{A_b}\{\varepsilon\}^T\{\sigma_1\}dA=\frac{1}{2}\{U\}^T[B]^T\{\sigma_1\}A_b; \quad (48)$$

$$\int_{A_b}\{\varepsilon\}^T[D]\left\{\varepsilon^*\right\}dA=\{U\}^T[B]^T[D]\left\{\varepsilon^*\right\}A_b=\{U\}^T\left\{F^*\right\}. \quad (49)$$

Steel shell is assumed to operate under momentless stress conditions, i.e. the FEs of the steel shell have only translational degrees of freedom, and rotational degrees of freedom are neglected. This hypothesis is valid for all points except corner zones in the absence of corner rounding. Real rectangular pipes have corner rounding, so this hypothesis can be considered for all points of the pipe. A linear approximation is adopted for axial displacements u of the shell FE:

$$u(s)=u_1+\frac{u_2-u_1}{l}s. \quad (50)$$

The circumferential deformation of the steel pipe is determined as the derivative of the displacement:

$$\varepsilon_{s\theta}=\frac{du}{ds}=\left[-\frac{1}{l}\frac{1}{l}\right]\begin{Bmatrix}u_1\\u_2\end{Bmatrix}=[B_s]\{U_s\}. \quad (51)$$

The stresses in the steel shell can be written based on (9)–(11) as:

$$\sigma_{s\theta}=\frac{E_s}{1-\nu_s^2}\left(\varepsilon_{s\theta}+\nu_s\left(\varepsilon_z^0+y_s\chi_1+x_s\chi_2\right)\right); \quad (52)$$

$$\sigma_{sz}=\frac{E_s}{1-\nu_s^2}\left(\varepsilon_z^0+y_s\chi_1+x_s\chi_2+\nu_s\varepsilon_{s\theta}\right). \quad (53)$$

Coordinates x_s and y_s change within the FE, but for simplicity it is proposed to calculate them at the FE center of gravity. The potential strain energy of the steel shell FE is determined as follows:

$$\prod_s=\frac{1}{2}\left(\delta\int_0^l\sigma_{s\theta}\varepsilon_{s\theta}ds+\delta\int_0^l\sigma_{sz}\varepsilon_{sz}ds\right). \quad (54)$$

Let us expand the first integral in (54):

$$\int_0^l \sigma_{s\theta}\varepsilon_{s\theta}ds = \frac{E_s}{1-\nu_s^2}\int_0^l \left(\left\{U_s\right\}^T\left[B_s\right]^T + \nu_s\left(\varepsilon_z^0 + y_s\chi_1 + x_s\chi_2\right)\right)\left[B_s\right]\left\{U_s\right\}ds =$$

$$= \frac{E_s l}{1-\nu_s^2}\left\{U_s\right\}^T\left[B_s\right]^T\left[B_s\right]\left\{U_s\right\} + \frac{E_s\nu_s l}{1-\nu_s^2}\left(\varepsilon_z^0 + y_s\chi_1 + x_s\chi_2\right)\left[B_s\right]\left\{U_s\right\} = \quad (55)$$

$$= \frac{1}{\delta}\left(\left\{U_s\right\}^T\left[K_s\right]\left\{U_s\right\} + \left\{U_s\right\}^T\left[B_s\right]^T\frac{E_s\nu_s l}{1-\nu_s^2}\left(\varepsilon_z^0 + y_s\chi_1 + x_s\chi_2\right)\right),$$

where $\left[K_s\right] = \frac{E_s\delta l}{1-\nu_s^2}\left[B_s\right]^T\left[B_s\right] = \frac{E_s\delta}{l\left(1-\nu_s^2\right)}\begin{bmatrix}1 & -1\\ -1 & 1\end{bmatrix}$ is the stiffness matrix of the steel shell FE.

Next, we expand the second integral in (54):

$$\int_0^l \sigma_{sz}\varepsilon_{sz}ds = \frac{E_s}{1-\nu_s^2}\int_0^l \left(\varepsilon_z^0 + y_s\chi_1 + x_s\chi_2 + \nu_s\left\{U_s\right\}^T\left[B_s\right]^T\right)\left(\varepsilon_z^0 + y_s\chi_1 + x_s\chi_2\right)ds =$$

$$= \frac{E_s}{1-\nu_s^2}\left(\int_0^l \left(\varepsilon_z^0 + y_s\chi_1 + x_s\chi_2\right)^2 ds + \nu_s\int_0^l \left(\varepsilon_0 + y_s\chi_1 + x_s\chi_2\right)\left[B_s\right]\left\{U_s\right\}ds\right). \quad (56)$$

The first integral in (56) vanishes after differentiation with respect to the vector of nodal displacements $\left\{U\right\}$. The second integral in (56) can be written in the following form:

$$\frac{E_s\nu_s}{1-\nu_s^2}\int_0^l \left(\varepsilon_0 + y_s\chi_1 + x_s\chi_2\right)\left[B_s\right]\left\{U_s\right\}ds = \left\{U_s\right\}^T\left[B_s\right]^T\frac{E_s\nu_s l}{1-\nu_s^2}\left(\varepsilon_z^0 + y_s\chi_1 + x_s\chi_2\right). \quad (57)$$

The work of external loads on the column displacements in the xy plane is equal to zero. Consequently, the Lagrange functional for the problem under consideration is equivalent to the potential strain energy. Differentiation of the expression for the potential strain energy by the vector of nodal displacements $\left\{U\right\}$ leads to the following system of equations:

$$\left[K\right]\left\{U\right\} + \left\{F_b\right\} + \left\{F_s\right\} - \left\{F^*\right\} = 0, \quad (58)$$

where $\left[K\right] = \left[K_b\right] + \left[K_s\right]$,

$$\left\{F_b\right\} = \left[B\right]^T\left\{\sigma_1\right\}A_b = \left[B\right]^T A_b\frac{E_1\nu_1}{1-\nu_1^2}\left(\varepsilon_z^0 + y_s\chi_1 + x_s\chi_2 - \varepsilon_z^*\right)\begin{Bmatrix}1\\1\\0\end{Bmatrix}; \quad (59)$$

$$\left\{F_s\right\} = \left[B_s\right]^T\frac{E_s\delta\nu_s l}{1-\nu_s^2}\left(\varepsilon_z^0 + y_s\chi_1 + x_s\chi_2\right). \quad (60)$$

The vector $\left\{F_s\right\}$ in (60), as well as the matrix $\left[K_s\right]$ in (55) are written in the local coordinate system of the steel shell FE. When forming the system of equations of the FE method for the entire section, it is necessary to transform matrices and vectors from local coordinate systems to the global one using the formulas:

$$\left\{\overline{U}\right\} = \left[L\right]\left\{U\right\}; \quad (61)$$

$$\left[K\right] = \left[L\right]^T\left[\overline{K}\right]\left[L\right]; \quad (62)$$

$$\{F\} = [L]^T \{\bar{F}\}; \tag{63}$$

$$[L] = \begin{bmatrix} \cos\alpha & \sin\alpha & 0 & 0 \\ 0 & 0 & \cos\alpha & \sin\alpha \end{bmatrix}. \tag{64}$$

The bar above the vectors and matrices in formulas (61)–(63) corresponds to the local coordinate system.

To take into account the thickness of the pipe wall when calculating the stiffness in formulas (17)–(25), matrices $[K_s]$ and vectors $\{F_s\}$, nodal coordinates of the steel shell are reduced to the middle of the wall thickness according to the formulas:

$$x_p = x_b \cdot \frac{B-\delta}{B_b}; \tag{65}$$

$$y_p = y_b \cdot \frac{H-\delta}{H_b}, \tag{66}$$

where x_b and y_b are the coordinates of the node on the contour of the concrete core, x_p and y_p are the coordinates of the node on the center line of the pipe wall, B_b and H_b are the dimensions of the concrete core.

The system of equations (58) allows to calculate the stresses σ_x, σ_y, τ_{xy}, as well as $\sigma_{s\theta}$ in the plane of the cross section using the values of generalized deformations ε_z^0, χ_1 and χ_2.

The equations of the concrete deformation theory of plasticity by G.A. Geniyev [28] are used as a model of the material for concrete. In these equations, the dilation effect is taken into account by introducing the value of dilation deformation ε_d. The value ε_d is determined by the formula:

$$\varepsilon_d = -\frac{g_0 \Gamma^2}{3}, \tag{67}$$

where g_0 is the dilation modulus, $\Gamma = \sqrt{\frac{2}{3}}\sqrt{(\varepsilon_1-\varepsilon_2)^2+(\varepsilon_2-\varepsilon_3)^2+(\varepsilon_1-\varepsilon_3)^2}$ is the intensity of shear deformations.

Dilatational deformation can be considered a special case of forced deformation $\left(\varepsilon_x^* = \varepsilon_y^* = \varepsilon_z^* = \varepsilon_d,\ \gamma_{xy}^* = 0\right)$. The adopted stress-strain diagram for steel is a diagram of ideal elastic-plastic material with the Huber–Mises–Hencky yield criterion.

The calculation taking into account physical nonlinearity is performed according to a scheme with a stepwise increase in load in the following sequence:

1. At the first step of loading, the modulus of elasticity of concrete and steel are taken equal to the initial values corresponding to the elastic work of the material. Dilatational deformations are absent at the first step.
2. Cross-section stiffness matrix $[D_1] = \begin{bmatrix} EA & ES_x & ES_y \\ ES_x & EI_x & EI_{xy} \\ ES_y & EI_{xy} & EI_y \end{bmatrix}$ and vector $\begin{Bmatrix} \Delta N^* \\ \Delta M_x^* \\ \Delta M_y^* \end{Bmatrix}$ are calculated using formulas (12).
3. The increments of generalized deformations are determined by the formula:

$$\{\Delta\varepsilon\} = \begin{Bmatrix} \Delta\varepsilon_z^0 \\ \Delta\chi_1 \\ \Delta\chi_2 \end{Bmatrix} = [D_1]^{-1} \cdot \{\Delta F\}, \quad (68)$$

where $\{\Delta F\} = \left(\begin{Bmatrix} \Delta N \\ \Delta M_x \\ \Delta M_y \end{Bmatrix} + \begin{Bmatrix} \Delta N^* \\ \Delta M_x^* \\ \Delta M_y^* \end{Bmatrix} \right)$.

1. The stress-strain state in the plane of the cross section is determined based on the values of generalized deformations using the system of equations (58).
2. The tangential elastic moduli of concrete and steel are corrected based on the calculated stresses and deformations.
3. The corrected matrix $[D_1']$ and the residual vector of forces $\{\delta F\} = \{\Delta F\} - [D_1']\{\Delta\varepsilon\}$ are calculated.
4. Vector of additional deformations $\{\delta\varepsilon\} = [D_1']^{-1}\{\Delta F\}$ caused by the discrepancy of forces is determined.
5. The vector $\{\Delta\varepsilon\}$ is corrected according to the formula $\{\Delta\varepsilon\} := \{\Delta\varepsilon\} + \{\delta\varepsilon\}$.
6. Steps 3–6 are repeated in approximations from the second to $j_{\max}$, where $j_{\max}$ is the maximum number of iterations. Starting from the second iteration, convergence is controlled using the formula:

$$\frac{\left\| \{\delta\varepsilon_j\} - \{\delta\varepsilon_{j-1}\} \right\|}{\left\| \{\delta\varepsilon_j\} \right\|} \cdot 100\% < 0.1\%, \quad (69)$$

where $\|\{a\}\| = \sqrt{\{a\}^T \{a\}}$ is the vector norm.

Each loading step ends with the calculation of total deformations and stresses, as well as recalculation of stiffness matrices.

The described calculation algorithm was implemented by the authors in the MATLAB environment.

3. Results and Discussion

At the first stage, the developed method was compared in an elastic setting with the results of a three-dimensional analysis in the ANSYS 2021R1 software package. The eccentrically compressed CFST column with the cross-sectional size of 300×200 mm, length of 2000 mm, and wall thickness of 5.73 mm was considered. A concentrated force F = 1 kN was applied at the corner of the cross-section (Fig. 3). The column had a fixed support at the bottom. To eliminate local effects at the upper end caused by the action of the concentrated force, the 10 mm thick metal rigid plate was installed on top, which in ANSYS Workbench was set as “Surface Coating”. Surface Coating objects are the shell FEs whose nodes coincide with the nodes of volumetric FEs located on the surface of the concrete core. Stiffness behavior for the plate on the upper end was taken as “Membrane and Bending”. The steel pipe was also modeled with “Surface Coating” objects with stiffness behavior “Membrane Only”. This stiffness behaviour was adopted to eliminate local effects caused by bending moments at the corners of the rectangular tube. The concrete core was modeled using FEs in the form of parallelepipeds. The FE mesh size was taken to be 10 mm.

Since the steel pipe was defined by “Surface Coating” objects, then when modeling using the author's method, it was simply assumed that $B = B_b$, $H = H_b$, and formulas (42) were not used.

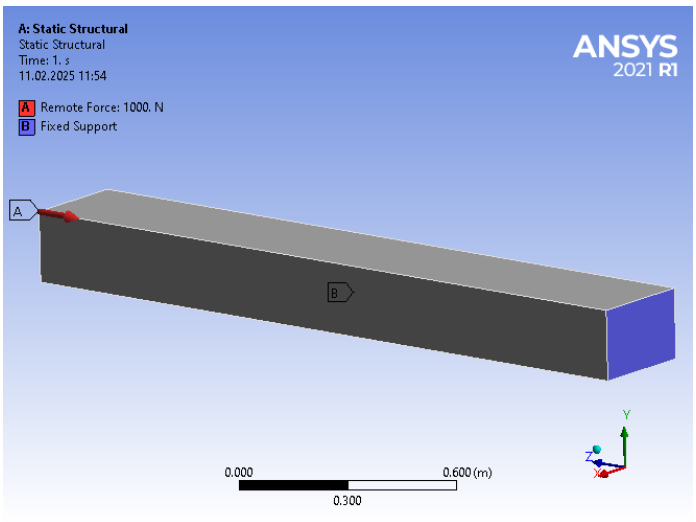

Figure 3. Calculation scheme in ANSYS.

Figs. 4, 5 show the stresses σ_z isofields for concrete in the middle section $\left(z = L/2\right)$, obtained as a result of three-dimensional modeling in ANSYS and using a simplified method proposed by the authors. The highest tensile stresses were 32.16 kPa when calculated in ANSYS and 32.58 kPa when calculated using the author's method. The highest compressive stresses were 52.08 kPa when calculated in ANSYS and 52.04 kPa when calculated using the author's method.

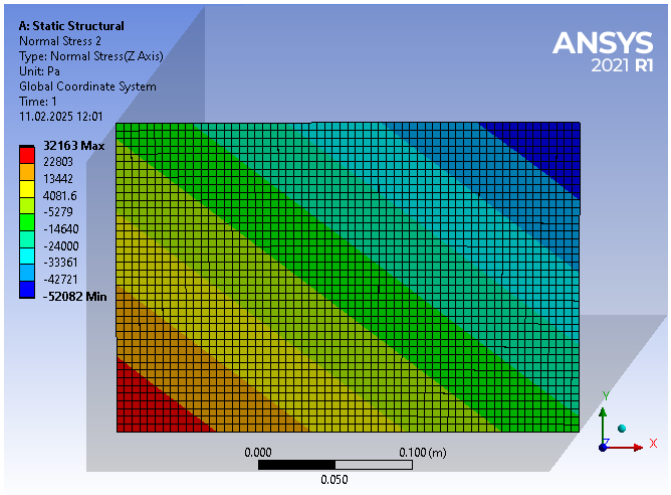

Figure 4. Stress isofields σ_z (Pa) in ANSYS.

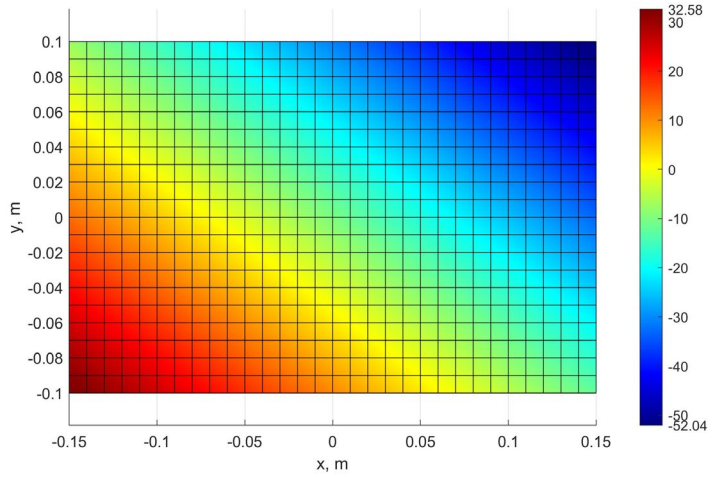

Figure 5. Isofields of stresses σ_z (kPa), obtained using the author's method.

Figs. 6, 7 show the stresses σ_x isofields in concrete obtained as a result of calculation in ANSYS and according to the author's method. Figs. 8, 9 are the same for stresses σ_y. The maximum stress σ_x value was 5.68 kPa in ANSYS and 5.81 kPa according to the author's method. The minimum stress σ_x value was –3.55 kPa in ANSYS and –3.54 kPa according to the author's method. The maximum and minimum stresses σ_y in the calculation with ANSYS coincided with the maximum and minimum stresses σ_x. When calculating according to the author's method, the maximum stress σ_y was 5.75 kPa, and the minimum was –3.49 kPa.

Thus, the greatest deviation of the calculation results using the author's method from the results in ANSYS is 2.3 %, and the average deviation is 0.5 %.

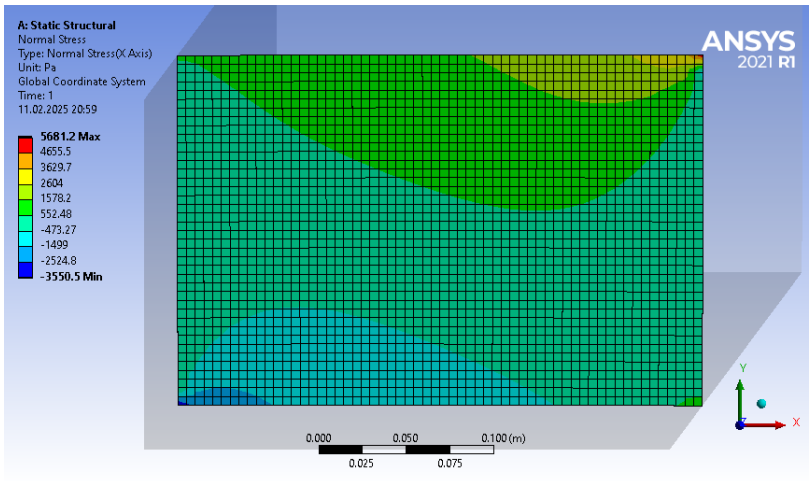

Figure 6. Isofields of stresses σ_x (Pa) in concrete core obtained in ANSYS.

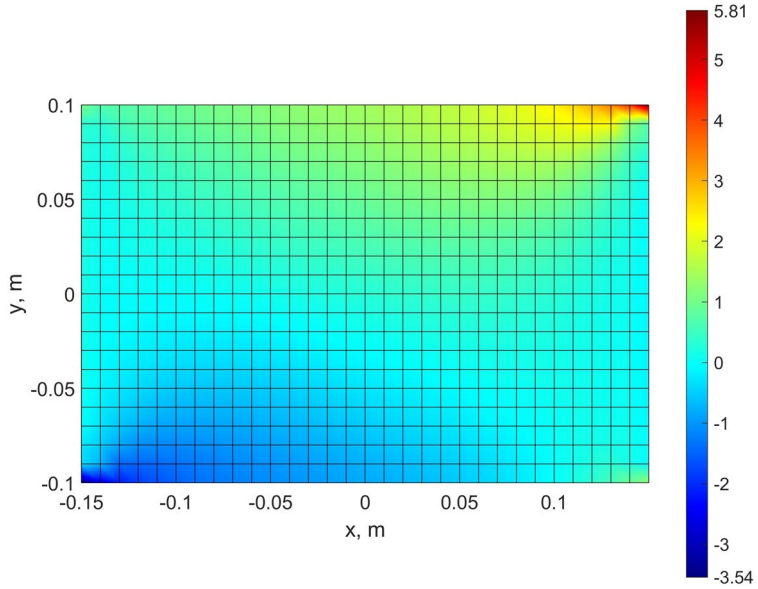

Figure 7. Isofields of stresses σ_x (kPa) in the concrete core, obtained using the author's method.

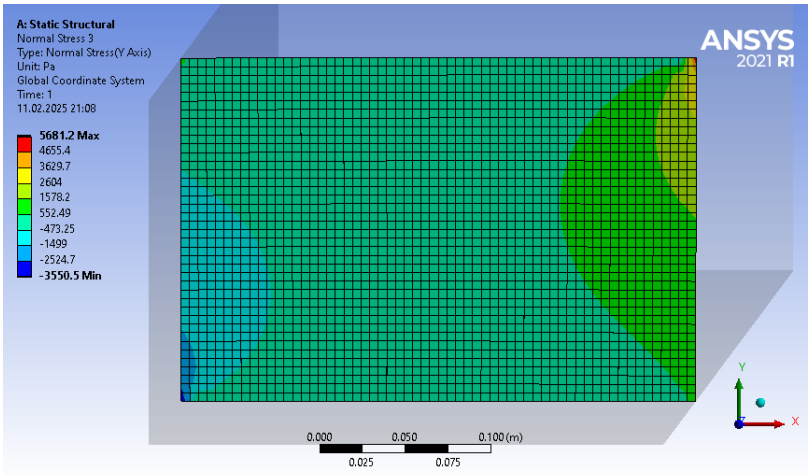

Figure 8. Isofields of stresses σ_y (Pa) in concrete core obtained in ANSYS.

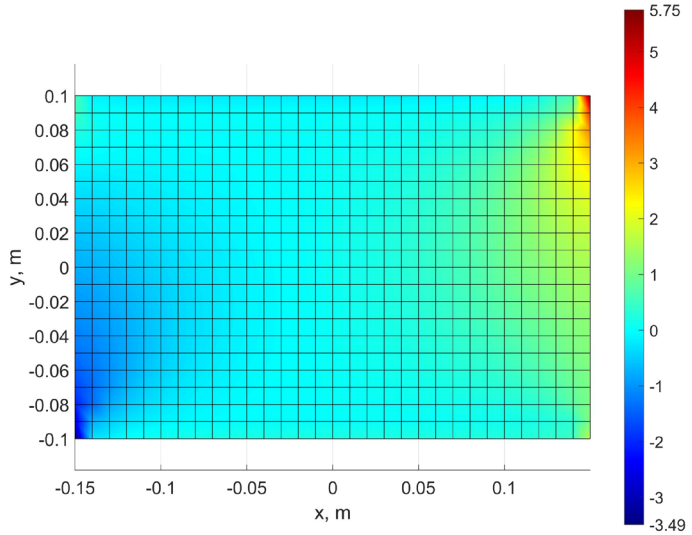

Figure 9. Isofields stresses σ_y (kPa) in the concrete core, obtained using the author's method.

The developed method was also tested on experimental data for 38 samples given in [29–31]. The experimental data included results for centrally compressed CFST columns, as well as for eccentrically compressed columns with eccentricity in one and two planes. Table 1 compares the calculation results according to the author's method in a physically nonlinear formulation with the experimental results. In this table, R_c is the compressive strength of concrete determined from tests of concrete cubes, $N_{\exp}$ and N_{calc} are respectively experimental and calculated values of the ultimate load.

Table 1. Comparison of calculation results with experimental data.

Sample	B, mm	H, mm	t, mm	R_c, MPa	R_y, MPa	e_x, mm	e_y, mm	N_{exp}, kN	N_{calc}, kN
B. Uy, 2001 [29]									
HSS1	110	110	5	28	750	0	0	1836	1834
HSS2	110	110	5	28	750	0	0	1832	1834
HSS3	110	110	5	30	750	15	0	1555	1431
HSS4	110	110	5	30	750	30	0	1281	1153
HSS8	160	160	5	30	750	0	0	2868	2 806
HSS9	160	160	5	30	750	0	0	2922	2806
HSS10	160	160	5	30	750	25	0	2024	2105
HSS11	160	160	5	30	750	50	0	1979	1662
HSS14	210	210	5	32	750	0	0	3710	42 05
HSS15	210	210	5	32	750	0	0	3483	4205
HSS16	210	210	5	32	750	25	0	3106	3292
HSS17	210	210	5	32	750	50	0	2617	2669

Sample	B, mm	H, mm	t, mm	R_c, MPa	R_y, MPa	e_x, mm	e_y, mm	N_{exp}, kN	N_{calc}, kN
Y. Yang et al., 2011 [30]									
Scfst-1	150	150	3	59.3	324	0	0	1618	1559
Scfst-2	150	150	3	59.3	324	15	0	1260	1260
Scfst-3	150	150	3	59.3	324	30	0	1244	1057
Scfst-4	150	150	3	59.3	324	15	15	1280	1195
Scfst-5	150	150	3	59.3	324	30	30	1193	925
Rcfst-1	180	120	3	59.3	324	0	0	1476	1517
Rcfst-2	180	120	3	59.3	324	36	0	1140	1020
Rcfst-3	180	120	3	59.3	324	18	12	1147	1160
Rcfst-4	180	120	3	59.3	324	36	24	939	900
X. Qu et al., 2013 [31]									
PYA-1	150	100	4.065	48.75	235	10	0	750	822
PYA-2	150	100	4.065	82.5	235	15	0	1040	1035
PYA-3	150	100	4.065	65	235	20	0	810	850
PYA-4	200	150	4.433	65	235	20	0	1750	1670
PYA-5	200	150	4.433	48.75	235	30	0	1250	1260
PYA-6	200	150	4.433	82.5	235	40	0	1400	1630
PYA-7	300	200	5.73	82.5	345	50	0	3450	3850
PYA-8	300	200	5.73	65	345	60	0	2650	3150
PYA-9	300	200	5.73	48.75	345	70	0	2445	2610
PYB-1	150	100	4.065	48.75	235	8.32	5.55	980	822
PYB-2	150	100	4.065	82.5	235	12.48	8.32	950	1039
PYB-3	150	100	4.065	65	235	16.64	11.09	980	838
PYB-4	200	150	4.433	65	235	16	12	1300	1683
PYB-5	200	150	4.433	48.75	235	24	18	1300	1275
PYB-6	200	150	4.433	82.5	235	32	24	1600	1588
PYB-7	300	200	5.73	82.5	345	38.41	32.01	3600	3740
PYB-8	300	200	5.73	65	345	46.09	38.41	2550	3020

The average value of the $N_{calc}/N_{\exp}$ ratio was 1.01, the maximum was 1.29, and the minimum was 0.78. The standard deviation was 0.11, and the coefficient of variation was 11 %.

4. Conclusions

A simplified method for determining the bearing capacity of eccentrically compressed rectangular CFST columns in the presence of axial force eccentricities in two planes has been developed. The proposed method allows reducing the three-dimensional problem of determining the stress-strain state to a two-dimensional one, which ensures significant savings in machine time. This allows calculation in a physically nonlinear formulation not only for individual elements, but also for buildings that include CFST elements as a whole.

The verification of the developed method was performed by comparison with the results of FEA of the three-dimensional model in an elastic formulation in the ANSYS software package using volumetric FEs for concrete and shell FEs for a steel pipe. The maximum deviation of the results for stresses was 2.3 %. Validation of the developed method was performed using experimental data for 38 samples presented in three different works.

It should be noted that the proposed method does not allow for the slippage of concrete in the steel pipe, local stability loss of the pipe wall and the separation of the concrete core from the steel shell. The first two factors can be taken into account only when analyzing the column in a three-dimensional formulation, which is a very labor-intensive process and is not suitable for analyzing entire buildings. The third factor can be taken into account in the approach we propose. To implement this, the FEs of the steel pipe must be given a third bending degree of freedom, and one-way connections must be established between the nodes of the concrete and the steel shell that work only in compression. The development of the proposed model in this direction is a prospect for our further research.

References

1. Chen, Z., Ning, F., Song, C., Liang, Y. Study on axial compression bearing capacity of novel concrete-filled square steel tube columns. Journal of Building Engineering. 2022. 51. Article no. 104298. DOI: 10.1016/j.jobe.2022.104298
2. Grzeszykowski, B., Szmigiera, E.D. Experimental Investigation on the Vertical Ductility of Rectangular CFST Columns Loaded Axially. Materials. 2022. 15(6). Article no. 2231. DOI: 10.3390/ma15062231
3. Moradi, M.J., Daneshvar, K., Ghazi-Nader, D., Hajiloo, H. The prediction of fire performance of concrete-filled steel tubes (CFST) using artificial neural network. Thin-Walled Structures. 2021. 161. Article no. 107499. DOI: 10.1016/j.tws.2021.107499
4. Ren, Z., Wang, D., Li, P. Axial compressive behaviour and confinement effect of round-ended rectangular CFST with different central angles. Composite Structures. 2022. 285. Article no. 115193. DOI: 10.1016/j.compstruct.2022.115193
5. Remya, K.V., Prasad, R. Comparison of Seismic Performance of Different Irregular High Rise Structures with RCC and CFST Columns. Lectures Notes in Civil Engineering. 607. Proceedings of SECON'24 (SECON 2024). Pp. 623–644. DOI: 10.1007/978-3-031-70431-4_45
6. Jiao, C., Liu, W., Li, Y., Shi, W., Long, P. Experimental study of CFST embedded precast concrete bridge column-foundation connection with studs. Soil Dynamics and Earthquake Engineering. 2023. 168. Article no. 107826. DOI: 10.1016/j.soildyn.2023.107826
7. Mander, J.B., Priestley, M.J., Park, R. Theoretical Stress-Strain Model for Confined Concrete. Journal of Structural Engineering. 1988. 114(8). Pp. 1804–1826. DOI: 10.1061/(ASCE)0733-9445(1988)114:8(1804)
8. Yu, T.T.J.G., Teng, J.G., Wong, Y.L., Dong, S.L. Finite element modeling of confined concrete-I: Drucker-Prager type plasticity model. Engineering Structures. 2010. 32(3). Pp. 665–679. DOI: 10.1016/j.engstruct.2009.11.014
9. Ding, F., Cao, Z., Lyu, F., Huang, S., Hu, M., Lin, Q. Practical design equations of the axial compressive capacity of circular CFST stub columns based on finite element model analysis incorporating constitutive models for high-strength materials. Case Studies in Construction Materials. 2022. 16. Article no. e01115. DOI: 10.1016/j.cscm.2022.e01115
10. Sarir, P., Jiang, H., Asteris, P.G., Formisano, A., Armaghani, D.J. Iterative Finite Element Analysis of Concrete-Filled Steel Tube Columns Subjected to Axial Compression. Buildings. 2022. 12(12). Article no. 2071. DOI: 10.3390/buildings12122071
11. Megahed, K., Mahmoud, N.S., Abd-Rabou, S.E.M. Finite Element Modeling for Concrete-Filled Steel Tube Stub Columns under Axial Compression. International Journal of Steel Structures. 2024. 24(5). Pp. 1229–1250. DOI: 10.1007/s13296-024-00896-7
12. Wang, F.C., Xie, W.Q., Li, B., Han, L.H. Experimental study and design of bond behavior in concrete-filled steel tubes (CFST). Engineering Structures. 2022. 268. Article no. 114750. DOI: 10.1016/j.engstruct.2022.114750
13. Wang, S., Wang, W., Xie, Z. Nonlinear cyclic behavior of steel tube in concrete-filled steel tube members including local buckling. Thin-Walled Structures. 2023. 191. Article no. 111055. DOI: 10.1016/j.tws.2023.111055
14. Ahmed, M., Sheikh, M.N., Hadi, M.N., Liang, Q.Q. Nonlinear analysis of square spiral-confined reinforced concrete-filled steel tubular short columns incorporating novel confinement model and interaction local buckling. Engineering Structures. 2023. 274. Article no. 115168. DOI: 10.1016/j.engstruct.2022.115168
15. Almasabha, G., Ramadan, M. Finite Element Modelling of Circular Concrete-Filled Steel Tubular Columns Under Quasi-Static Axial Compression Loading. Journal of Composites Science. 2024. 8(11). Article no. 472. DOI: 10.3390/jcs8110472
16. Nakahara, H., Uchida, K., Yanai, Y. Test and Analysis for Shearing Behavior of Circular CFST Columns. Buildings. 2024. 14(12). Article no. 3871. DOI: 10.3390/buildings14123871
17. Yadav, R., Chen, B. Parametric Study on the Axial Behaviour of Concrete Filled Steel Tube (CFST) Columns. American Journal of Applied Scientific Research. 2017. 3(4). Pp. 37–41. DOI: 10.11648/j.ajasr.20170304.11
18. Manikandan, K.B., Umarani, C. Parametric study of CFST columns by numerical mock-up. Materials Today: Proceedings. 2021. 45(7). Pp. 6021–6027. DOI: 10.1016/j.matpr.2020.09.532
19. Xu, L., Pan, J., Yang, X. Mechanical performance of self-stressing CFST columns under uniaxial compression. Journal of Building Engineering. 2021. 44. Article no. 103366. DOI: 10.1016/j.jobe.2021.103366
20. Reddy, G.S.R., Bolla, M., Patton, M.L., Adak, D. Comparative study on structural behaviour of circular and square section-Concrete Filled Steel Tube (CFST) and Reinforced Cement Concrete (RCC) stub column. Structures. 2021. 29. Pp. 2067–2081. DOI: 10.1016/j.istruc.2020.12.078
21. Erdoğan, A., Güneyisi, E.M., İpek, S. Finite Element Modelling of Ultimate Strength of CFST Column and Its Comparison with Design Codes. Bilecik Şeyh Edebali Üniversitesi Fen Bilimleri Dergisi. 2022. 9(1). Pp. 324–339. DOI: 10.35193/bseufbd.1033827
22. Hou, C., Zhou, X.G. Strength prediction of circular CFST columns through advanced machine learning methods. Journal of Building Engineering. 2022. 51. Article no. 104289. DOI: 10.1016/j.jobe.2022.104289
23. Le, T.T. Practical machine learning-based prediction model for axial capacity of square CFST columns. Mechanics of Advanced Materials and Structures. 2022. 29(12). Pp. 1782–1797. DOI: 10.1080/15376494.2020.1839608
24. Zarringol, M., Thai, H.T. Prediction of the load-shortening curve of CFST columns using ANN-based models. Journal of Building Engineering. 2022. 51. Article no. 104279. DOI: 10.1016/j.jobe.2022.104279
25. Đorđević, F., Kostić, S.M. Practical ANN prediction models for the axial capacity of square CFST columns. Journal of Big Data. 2023. 10(1). Article no. 67. DOI: 10.1186/s40537-023-00739-y
26. Chepurnenko, A.S., Turina, V.S., Akopyan, V.F. Artificial Intelligence Model for Predicting the Load-Bearing Capacity of Eccentrically Compressed Short Concrete Filled Steel Tubular Columns. Construction Materials and Products. 2024. 7(2). Article no. 2. DOI: 10.58224/2618-7183-2024-7-2-2
27. Chepurnenko, A., Yazyev, B., Meskhi, B., Beskopylny, A., Khashkhozhev, K., Chepurnenko, V. Simplified 2D Finite Element Model for Calculation of the Bearing Capacity of Eccentrically Compressed Concrete-Filled Steel Tubular Columns. Applied Sciences. 2021. 11(24). Article no. 11645. DOI: 10.3390/app112411645
28. Litvinov, S.V., Yazyev, B.M., Kuznetsov, V.V., Belyugin, N.V., Avakov, A.A. Study of the concordance between various concrete deformation models and experimental data for uniaxial compression cases. Construction Materials and Products. 2024. 7(6). Article no. 6. DOI: 10.58224/2618-7183-2024-7-5-6
29. Uy, B. Strength of short concrete filled high strength steel box columns. Journal of Constructional Steel Research. 2001. 57(2). Pp. 113–134. DOI: 10.1016/S0143-974X(00)00014-6

30. Yang, Y.F., Han, L.H. Behaviour of concrete filled steel tubular (CFST) stub columns under eccentric partial compression. Thin-Walled Structures. 2011. 49(2). Pp. 379–395. DOI: 10.1016/j.tws.2010.09.024
31. Qu, X., Chen, Z., Sun, G. Experimental study of rectangular CFST columns subjected to eccentric loading. Thin-Walled Structures. 2013. 64. Pp. 83–93. DOI: 10.1016/j.tws.2012.12.006

Information about the authors:

***Anton Chepurnenko**, Doctor of Technical Sciences*
ORCID: https://orcid.org/0000-0002-9133-8546
E-mail: anton_chepurnenk@mail.ru

***Batyr Yazyev**, Doctor of Technical Sciences*
ORCID: https://orcid.org/0000-0002-5205-1446
E-mail: ps62@yandex.ru

***Samir Al-Zgul**,*
ORCID: https://orcid.org/0000-0001-6182-786X
E-mail: samiralzgulfx@gmail.com

***Vasilina Tyurina**, PhD in Technical Sciences*
ORCID: https://orcid.org/0009-0001-6399-401X
E-mail: vasilina.93@mail.ru

Received 21.01.2025. Approved after reviewing 23.03.2025. Accepted 23.03.2025.